UC Irvine

Title

Leaf Area Index Estimates Using Remotely Sensed Data and BRDF Models in a Semiarid Region

Authors

Qi, J
Kerr, YH
Moran, MS
et al.

Peer reviewed

Leaf Area Index Estimates Using Remotely Sensed Data and BRDF Models in a Semiarid Region

J. Qi,* Y. H. Kerr†, M. S. Moran,* M. Weltz,‡ A. R. Huete,§ S. Sorooshian,¶ and R. Bryant*

*T*he amount and spatial and temporal dynamics of vegetation are important information in environmental studies and agricultural practices. There has been a great deal of interest in estimating vegetation parameters and their spatial and temporal extent using remotely sensed imagery. There are primarily two approaches to estimating vegetation parameters such as leaf area index (LAI). The first one is associated with computation of spectral vegetation indices (SVI) from radiometric measurements. This approach uses an empirical or modeled LAI–SVI relation between remotely sensed variables such as SVI and biophysical variables such as LAI. The major limitation of this empirical approach is that there is no single LAI-SVI equation (with a set of coefficients) that can be applied to remote-sensing images of different surface types. The second approach involves using bidirectional reflectance distribution function (BRDF) models. It inverts a BRDF model with radiometric measurements to estimate LAI using an optimization procedure. Although this approach has a theoretical basis and is potentially applicable to varying surface types, its primary limitation is the lengthy computation time and difficulty of obtaining the required input parameters by the model. In this study, we present a strategy that combines BRDF models and conventional LAI–SVI approaches to circumvent these limitations. The proposed strategy was implemented in three sequential steps. In the first step, a BRDF model was inverted with a limited number of data points or pixels to produce a training data set consisting of leaf area index and associated pixel values. In the second step, the training data set passed through a quality control procedure to remove outliers from the inversion procedure. In the final step, the training data set was used either to fit an LAI–SVI equation or to train a neural fuzzy system. The best fit equation or the trained fuzzy system was then applied to large-scale remote-sensing imagery to map spatial LAI distribution. This approach was applied to Landsat TM imagery acquired in the semiarid southeast Arizona and AVHRR imagery over the Hapex-Sahel experimental sites near Niamy, Niger. The results were compared with limited ground-based LAI measurements and suggested that the proposed approach produced reasonable estimates of leaf area index over large areas in semiarid regions. This study was not intended to show accuracy improvement of LAI estimation from remotely sensed data. Rather, it provides an alternative that is simple and requires little knowledge of study target and few ground measurements. ©Elsevier Science Inc., 2000

* USDA-ARS Water Conservation Laboratory, Phoenix
† CESBIO, CNES, Toulouse, France
‡ USDA-ARS Great Plains System Research, Ft. Collins, Colorado
§ Department of Soil, Water, and Environmental Sciences, University of Arizona, Tucson
¶ Department of Hydrology and Water Resources, University of Arizona, Tucson

Address correspondence to J. Qi, Dept. of Geography, Michigan State Univ. East Lansing, MI 48824-1115. E-mail: qi@pilot.msu.edu or qi@tucson.ars.ag.gov

INTRODUCTION

Although remotely sensed data are becoming more available, operational algorithms or procedures to convert radiometric measurements into biophysical variables, such as LAI, are still in their infancy. There are two common approaches to estimating LAI using remote-sensing imagery: a vegetation index (VI) approach and a modeling approach. The VI approach is associated with spectral

vegetation indices (SVI) such as the normalized difference vegetation index (NDVI):

$$\text{NDVI} = (\rho_{\text{NIR}} - \rho_{\text{Red}})/(\rho_{\text{NIR}} + \rho_{\text{Red}}), \qquad (1)$$

where ρ is spectral reflectance in the red and near-infrared (NIR) region. A common procedure to estimate LAI is to establish an empirical relationship between NDVI and LAI by statistically fitting observed LAI values to the corresponding NDVI. Among proposed LAI–SVI relations are the following forms (Baret, 1995; Best and Harlan, 1985; Curran, 1983; Asrar et al., 1985a,b; Peterson et al., 1987; Price and Bausch, 1995):

$$\text{LAI} = ax^3 + bx^2 + cx + d, \qquad (2)$$

$$\text{LAI} = a + bx^c, \qquad (3)$$

$$\text{LAI} = -1/2a\ \ln(1-x), \qquad (4)$$

$$\text{LAI} = f(x), \qquad (5)$$

where x is either vegetation indices or reflectances derived from remotely sensed data. Coefficients a, b, c, and d are empirical parameters and vary with vegetation types. The last equation is a generic function of any form. Given a set of coefficients, the equations can be applied to remotely sensed images to map the spatial LAI distributions. The advantage of this approach is its simplicity and ease of computation.

A major limitation of this VI approach, however, is the diversity of the proposed LAI–SVI equations. These equations vary not only in mathematical form (linear, power, exponential, etc.), but also in their empirical coefficients, depending primarily on vegetation type. To operationally use this VI approach, an LAI–SVI equation must be established for each vegetation type, which requires substantial LAI measurements and corresponding remote-sensing data. Because there is no universal LAI–SVI equation applicable to diverse vegetation types, it is difficult to use this approach with large-scale remote-sensing images.

Another limitation of this approach is the sensitivity of SVI to nonvegetation related factors such as soil background properties (e.g., Huete, 1989; Qi et al., 1993), atmospheric conditions (e.g., Kaufman, 1989; Vermote et al., 1990), topography (Holben and Justice, 1980; Justice et al., 1981; Pinter et al., 1987), and bidirectional nature of surfaces (Kimes et al., 1985; Deering, 1989; Jackson et al., 1990; Roujean et al., 1992; Burgess and Pairman, 1997). The effects from soil background variations and atmospheric conditions may be minimized by developing improved vegetation indices (Huete, 1988; Clevers, 1989; Kaufman and Tanré, 1992; Qi et al., 1994a,b,c). The influence of Sun–surface–sensor geometry needs to be incorporated in vegetation index development and has not been done yet.

An alternative to empirical relationships is a modeling approach based on a set of radiative transfer equations or models. It involves inverting a model, $r = f$ (LAI, ...), where LAI is an input parameter to the model and r is the model output (reflectances, or radiance). Model inversion is a process in which the model is run in a reverse mode, that is, the inputs to the inversion procedure are the reflectances (r) and the output is a set of the parameters. The technique commonly used to invert a model is to adjust the model parameters in such a way that the model-predicted values closely match the measured values (e.g., Pinty et al., 1990; Goel and Thompson, 1984a–b). Most commonly used models are bidirectional reflectance distribution function (BRDF) models. A BRDF model usually consists of a set of equations that relate surface physical properties to the observed signals as a function of wavelength. The physical properties may include soil reflectances, canopy architectures and optical properties, geometric configuration of the sensing systems, as well as the illumination sources. These properties are all necessary input parameters required by BRDF models. Some models may require other input parameters such as single scattering albedos of individual leaves, leaf inclination distribution, and anisotropic properties of both canopy and soil substrates. Given necessary inputs, bidirectional reflectances can be simulated. If bidirectional reflectances are available, BRDF models can theoretically be inverted to obtain the model parameters, and some vegetation properties can thus be estimated (Goel and Thompson, 1984a,b; Goel and Deering, 1985; Goel and Grier, 1987; Jacquemoud, 1993; Jacquemoud et al., 1995; Qi et al., 1995; Running et al., 1996).

A major advantage of the modeling approach is that it is a physically based approach and is independent of vegetation type. It only requires multidirectional measurements, which are available from many sensors such as AVHRR, VEGETATION, MODIS, and MISR.

There are two major limitations in operational use of a modeling approach with BRDF. The first one is related to the inversion process of a BRDF model. Some models may have multiple solutions, given a set of remote-sensing measurements, and the inversion may not always converge (Jacquemoud, 1993). This would result in unreliable estimates of biophysical variables. The second limitation is the computation time involved in a large number of inversion processes, which is a major barrier when using large satellite images.

In summary, both empirical and modeling approaches have advantages and limitations. The advantages of the empirical LAI–SVI approach are that it is simple and easy to compute. The limitations of this approach are related to variable LAI–SVI equations for different biomes, and a prior knowledge about the particular biomes is required in order to determine the empirical equation coefficients. The advantages of the modeling approach are that it is physically based and biome-independent. However, it requires substantial computation time for model inversion, and inversion may not always converge. Therefore, none of the approaches is desirable for operational applications. Consequently, the objective of this study is
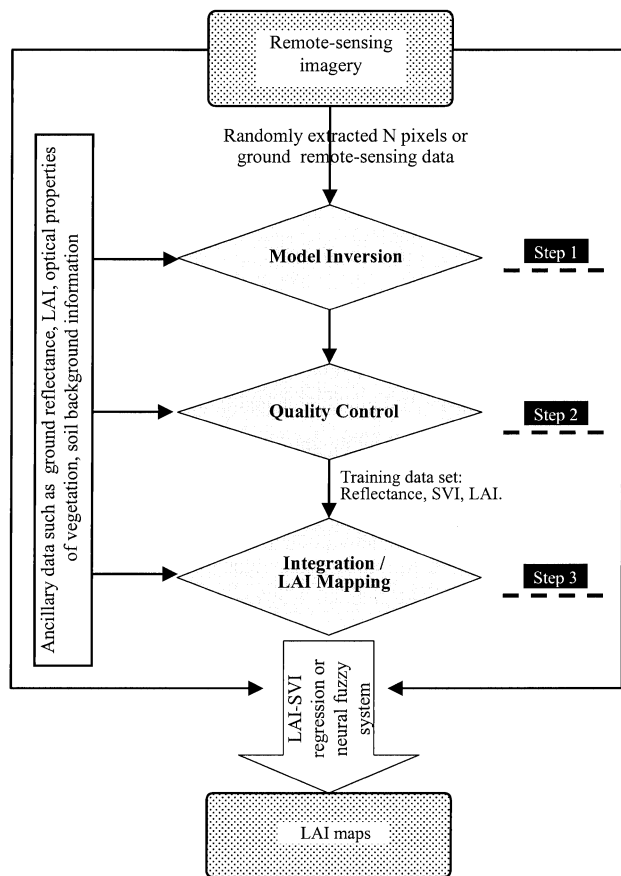
Figure 1. Graphic presentation of the proposed approach to estimating leaf area index with remote sensing imagery.

to develop an approach that has these advantages, but circumvents the limitations, thus enabling operational use of remotely sensed imagery to estimate vegetation densities.

METHODOLOGY

We designed an approach that combines the two approaches in such a way that the above-mentioned limitations can be circumvented, while taking advantage of easy computation of the LAI–SVI approach and physical aspects of the modeling approach. A graphic presentation of the proposed approach is illustrated in Figure 1. It consists of three sequential steps: model inversion, quality control, and integration/LAI mapping.

Step 1: Model Inversion

This is essentially the same as the modeling approach mentioned previously, except that it does not invert every single pixel or data point when applied to large-scale images. Instead, it randomly selects a limited number of pixels ($N=2500$ in this study) and uses them to perform an inversion process. Because the inversion is performed on a small number of data points, the computation time is greatly reduced, and the theoretical aspect of the mod-

eling approach is retained. The selected BRDF model in this study was the SAIL model by Verhoef (1984) because this model has been tested in many studies for LAI estimation using inversion techniques (e.g., Jacquemoud, 1993; Goel and Thompson, 1984a,b; Goel and Grier, 1987). The input parameters of this model include optical properties of leaves and background soil, canopy structure (leaf angle distribution: LAD), and canopy density (LAI). Given these parameters, the model can predict the reflectances. More discussions on model inversion can be found in other studies (Goel and Thompson 1984a,b; Goel and Grier, 1987; Goel and Deering, 1985; Jacquemoud, 1993; Qi et al., 1995). We used measured soil optical properties and ground multidirectional reflectance data to obtain leaf optical properties by inverting SAIL model. The spherical LAD distribution was determined to be the best among other distributions by examining the simulated reflectances against field measurements. Therefore, spherical LAD was used in this study, but can be treated as a free variable. The output of this step was the inverted LAI values of the randomly selected pixels and their corresponding reflectances and NDVI values. At this time, if any ancillary data such as measured LAD, leaf optical properties, or *in-situ* LAI measurements are available, they can be used either as inputs to the model for inversion or as output for the subsequent process.

Step 2: Quality Control

The parameters inverted in Step 1 are then passed to a quality control procedure, which checks the parameter boundary conditions to detect inversion failures. A failure occurs when the optimization algorithm does not find an optimal solution to the model before the boundary is reached. The boundary conditions can be defined by checking inverted LAI against observed values or against preset boundaries ($0 < LAI < LAI_{max}$), where LAI_{max} is the upper limit of LAI values of the study area. When a pixel fails in the inversion process or its inverted LAI reaches its boundaries, it is discarded. For example, if the inverted LAI value is negative or it exceeds the upper boundary, this pixel is then discarded. The purpose of this step was to eliminate outliers to avoid using them in the next step. The output of this step is called the training data set.

Step 3: Integration/LAI Mapping

Two integration/LAI mapping approaches can be used at this step. One is to use the training data set (from Step 2) to fit equations of the form $LAI = f(SVI)$ and another is to use a neural fuzzy inference system for LAI estimation.

LAI–SVI Approach
Once the data (LAI, SVI, and reflectance) pass through the quality control step, they are used to fit a suite of LAI-SVI equations proposed in the literature [Eqs. (2),

(3), (4), and (5)]. The purpose of this step is to find the optimal corresponding coefficients (obtained otherwise with field measurements) of those equations so that they can be applied to remote-sensing imagery. The technique used in the optimization in this study was to examine a statistical merit function δ^2, defined as

$$\delta^2 = \sum_{i=1}^{N} (LAI_e - LAI_m)^2, \qquad (6)$$

where subscript e stands for estimated LAI using the selected equation and subscript m stands for modeled LAI values from the inversion step. By examining the corresponding δ^2 values, the best-fit equation, along with its coefficients, is then used to map LAI distribution. This way, both the equation and its coefficients can be automatically obtained (instead of using published or field-measured values). This step takes advantage of the simplicity and easy computation of the LAI–SVI approach and circumvents the limitations of computation time of the modeling approach. Because only the selected equation is used, any outliers that accidentally passed through the quality control should be removed as well. We used the NDVI [Eq. (1)] for the LAI–SVI fitting because Eqs. (2)–(5) were proposed based on the NDVI analysis in their original studies. However, other vegetation indices, especially those that were designed to reduce different types of noise (Huete, 1988; Kaufman and Tanré, 1992; Pinty and Verstraete, 1992; Qi et al., 1994c), can be used.

Neural Fuzzy Logic Approach

An alternative to the LAI–SVI approach is to use techniques such as fuzzy inference system or neural network. To demonstrate the use of these techniques, we applied an adaptive-neural fuzzy inference system to investigate the feasibility of such a technique for operational applications of remote-sensing. The adaptive neural fuzzy inference routine was implemented in MATLAB®[1] software (ANFIS: adaptive neural fuzzy inference system). Use of this routine involved three steps: training the fuzzy system with a limited number of data points; checking the performance of the system with a separate data set; and then applying the trained system to remote-sensing imagery.

We used half of the data points that had passed through the quality control (Step 2) to train the ANFIS system and used the other half to check the system performance. The training and checking data sets included reflectances in the red and NIR spectral region, computed NDVI, and inverted LAI values. The trained fuzzy inference system was applied to remote-sensing images using the built-in procedure EVALFIS, which generated the best "guess" of LAI, given the input variables of red,

NIR, and NDVI. This procedure shortened the computation time substantially compared with the model inversion technique, although it took longer when compared with the LAI–SVI approach.

DATA DESCRIPTION

To test the proposed approaches, data sets from two field measurement campaigns were used to estimate spatial and temporal LAI patterns from satellite images. The first data set was obtained during the MONSOON'90 experiment (Kustas et al., 1991) conducted at the Walnut Gulch Experimental Watershed (31.72°N 110.68°W) near Tucson, Arizona in the summer of 1990. This watershed was representative of the brush and grass-covered rangeland found in a semiarid environment, and can be generally said to have only two seasons: dry and wet. Vegetation growth is triggered primarily by high-intensity thunderstorms, which normally occur in the wet season (July–October). The rest of the year is generally dry and the vegetation density is low (LAI<2.0).

During this campaign, ground- and aircraft-based bidirectional measurements (Huete et al., 1992; Qi et al., 1994b) were made over two sites, one dominated by desert grasses and the other by desert shrubs. Ground vegetation samples were collected near eight meteorological stations across the watershed. Although the dates of vegetation sampling did not coincide with remote-sensing measurements, the ground LAI data represented values of two seasons (dry and wet), which generally reflect the dynamics of vegetation densities of this region. Landsat TM images, having nearly nadir view angles, were acquired on 22 April and 7 September 1990. The raw digital images were converted to surface reflectance using ground-based reflectance measurements of known targets proposed by Moran et al. (1996). Together with airborne and ground measurements, these satellite images were applied to the proposed approach outlined in Figure 1 to map spatial and temporal LAI values.

The second data set included ground-based radiometric measurements at the Audubon research ranch, near Elgin, Arizona, coincident with LAI measurements. The dominant vegetation types were native upland grasses, Lehmann's lovegrass, and sacaton grasses. Radiometric measurements were made using an 8-band radiometer equipped with TM filters, by walking the radiometer along a preset transect. By ratioing the target readings to those measured over a reference panel, reflectance factors were computed. The *in-situ* LAI measurements were made with both destructive sampling and Li-Cor's LAI 2000 instrument. The instrument was calibrated against the data from destructive samples.

The third data set was from the Hapex-Sahel experiment in 1991–1992 near Niamey, Niger (Goutorbe et al., 1994; Prince et al., 1995; Kerr, 1994). The dominant vegetation types at two Super sites (13.24°N, 2.24°E and

---

[1] Trade names are included for the benefit of the reader and do not imply an endorsement of or a preference for the product listed by U.S. Department of Agriculture.

Table 1. Vegetation and Soil Optical Properties Obtained by Inversion of SAIL Model and Subsequently Used in This Study for LAI Mapping

Spectral Bands	Green	Red	NIR
Soil reflectance (ρ_S)	0.0967	0.1872	0.2327
Single leaf reflectance ($\rho_{\lambda L}$)	0.0970	0.2152	0.4459
Single leaf transmittance ($\tau_{\lambda L}$)	0.1085	0.1247	0.3478

13.54°N, 2.51°E) were agricultural crops and sparse shrubs interspersed with annual grasses and legumes. In this study, ground LAI measurements were made at South (Millet and Fallow) and Central West (Fallow) super sites. The LAI measurements of Fallow canopy were made in 1992, while those of Millet were made in 1993. Daily AVHRR images in 1992 were acquired and atmospheric corrections were made using the SMAC method (Rahman and Dedieu, 1994). Monthly composited AVHRR images were generated for May and September 1992 and applied to the equation derived in Step 3 (Figure 1) to map LAI spatial distributions. The LAI measurements of the Millet site were made only in 1993, when there was no coincident AVHRR imagery. The estimated LAI values from the 1992 imagery were used to compare with 1993 ground-LAI data instead in this study.

RESULTS

Equation Selected

Using the ground multidirectional measurements and inversion procedures, we obtained a set of parameters from the SAIL model ($\rho_{\lambda L}$, $\tau_{\lambda L}$, LAI, ρ_S), which are listed in Table 1. Parameters $\rho_{\lambda L}$ and $\tau_{\lambda L}$ are single leaf (L) reflectance and transmittance while ρ_S is the soil reflectance. They are all wavelength (λ)-dependent. Since these values are ob-

tained from inversion, they may differ from ground measurements. We suggest to use ground measurements, if available. Because of the similarity of vegetation types in the two experimental sites and in order to facilitate inversion process, the soil reflectance (ρ_S) and leaf optical properties ($\rho_{\lambda L}$, $\tau_{\lambda L}$) were assumed to be constant throughout the entire images once they were determined from the inversion step, while the LAI was allowed to vary. With these simplifications, randomly selected pixels (N=2500 pixels) from the TM image acquired on 7 September 1990 were used in the model inversion and computation of vegetation indices. The inverted LAI values, along with computed vegetation indices (NDVI), were then used for LAI–SVI equation selection. In this study, the selected equation based on the merit function [Eq. (6)] was the third-order polynomial equation [Eq. (2)] with the coefficients of a=18.99, b=−15.24, c=6.124, and d=−0.352. The fitting curve, plotted in Figure 2, was subsequently used as the LAI–SVI relation to produce an LAI map for all other remote-sensing images. For comparison purposes, a linear model proposed by Asrar et al. (1985b) also was plotted. Both the linear and polynomial curves fit the inverted LAI well at low density (LAI<1.2). The difference between the two approaches became significant with larger LAI values.

Adaptive Neural Fuzzy Inference System

The trained adaptive fuzzy system consisted of three inputs, each consisting of two generalized bell-shaped membership functions. The ANFIS consisted of eight linear membership functions. Because of the large number of training data points, the C-Means subtractive fuzzy inference system was used. This was to avoid placing equal weight on every data point in case the training data consist of unevenly distributed clusters. The perfor-
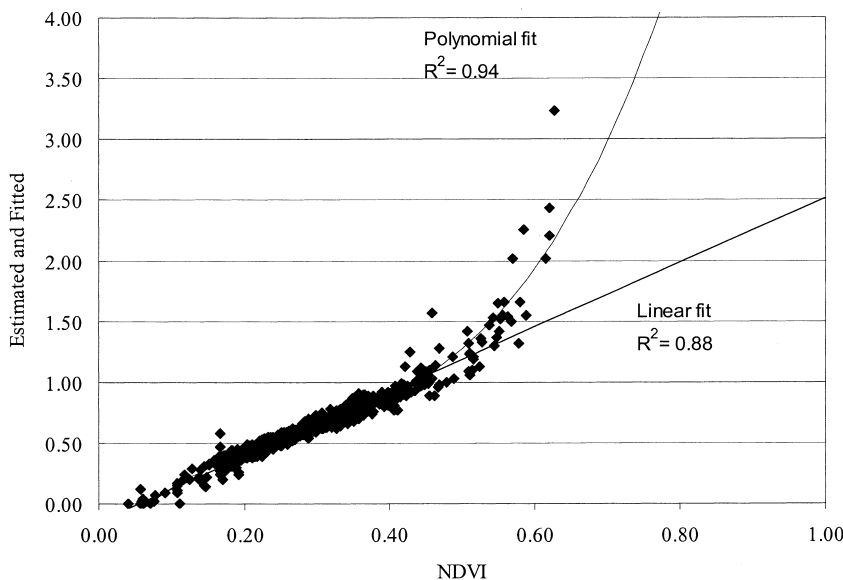

Figure 2. LAI–NDVI relationships [Eq. (2) in the text and a linear fit] used in this study.
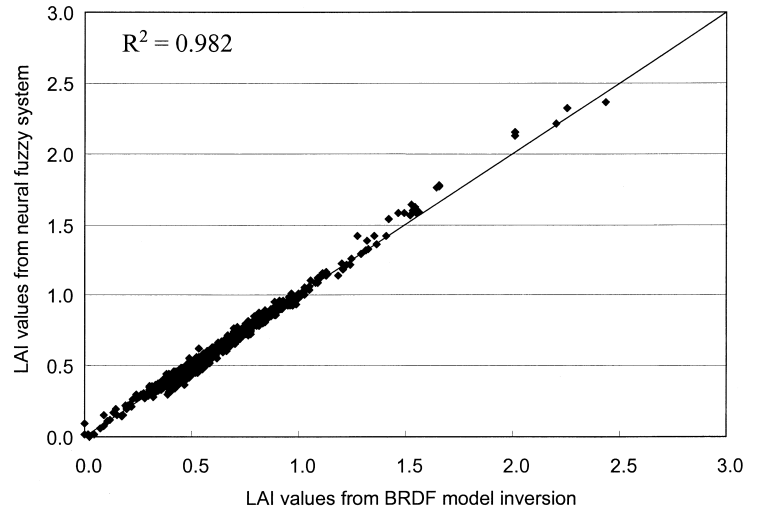
Figure 3. Performance of the neural fuzzy inference system. The *x*-axis is the training LAI values, while the *y*-axis is the output of the fuzzy system.

mance of the neural fuzzy system is presented graphically in Figure 3. The neural fuzzy inference system successfully predicted the LAI values.

LAI Estimation
The LAI maps for 22 April and 7 September 1990 (Fig. 4) were generated with the LAI–SVI equation [Eq. (2)] derived from TM subpixels in Step 3 (in Fig. 1). The estimated LAI values ranged from 0 to 0.8 on 22 April and from 0 to 3 on 7 September. The dark solid features were either roads or airstrips, and the white areas were streams where soil water content is generally greater because of accumulated rainfall. The approach produced LAI maps that agreed with the spatial distribution and temporal dynamics of the vegetation in this area.

The result of using the neural fuzzy system to map the LAI was demonstrated with the Landsat TM image acquired on 7 September 1990 (Fig. 5). The spatial pattern of the LAI map generated with the fuzzy inference system (Fig. 5a) was similar to that generated with the LAI–SVI equation (Fig. 5b). Statistical analysis (also see Fig. 3) indicated that there was no significant difference between the LAI maps generated with the neural fuzzy and LAI–SVI approaches. This suggests that the fuzzy inference system provided an easy and operationally feasible technique to apply sophisticated BRDF models to satellite images for LAI estimation (and possible other physical variables as well) over large areas.

The derived equation [Eq. (2)] was also applied to AVHRR images acquired at the Hapex-Sahel experiment site to test the applicability of the approach to larger scale remote-sensing imagery. The AVHRR had a spatial resolution of one kilometer. Figures 6a and 6b depict the dry and wet seasonal LAI patterns, derived from composited AVHRR images (11N–16°N, 0°E-5°E) of May and September 1992. The LAI maps showed the vegetation density gradient from south to north, due to precipitation differences of this region. The estimated LAI values ranged from 0 to 1.7 for the dry season and 0 to 2.8 for the wet season.

Comparison with Field Measurements
To validate the proposed approach, estimated LAI values using the derived equation [Eq. (2)] and satellite images were compared with field measurements. The comparison is presented in Figures 7 and 8. In Figure 7a, the LAI values estimated from TM images were compared with ground-based LAI values from eight meteorological stations across the Walnut Gulch Experimental Watershed. Because the ground LAI measurements were made on different dates, data acquired prior to 26 July were averaged to represent dry season vegetation density, and those data after this date were averaged to represent wet season vegetation density. The dry season ground measurements were compared with LAI values derived from 22 April TM images, while the wet season measurements were compared with those from 7 September TM images. Vegetation in this area is generally low for the entire period of dry season and then reaches a maximum standing biomass shortly after the monsoon season, which normally starts in late July. Although the TM-derived LAI values represent "snapshots" of dry and wet season, they agreed well with ground measurements. Because there was no coincident TM and ground LAI data available at this site, the results may not be conclusive.

To further validate the proposed approach, seasonal ground-based radiometric measurements were used to estimate LAI [using derived Eq. (2)] and compared with *in-situ* LAI measurements (Fig. 7b) made at the Audubon research ranch in 1997. At this site, paired ground radiometric and LAI measurements were available to allow a direct comparison. In Figure 7b, estimated LAI values using the linear LAI–SVI approach by Asrar et al. (1985b) was also included for comparison. The estimated LAI values with both linear and derived polynomial equations agreed well with the *in-situ* measurements.
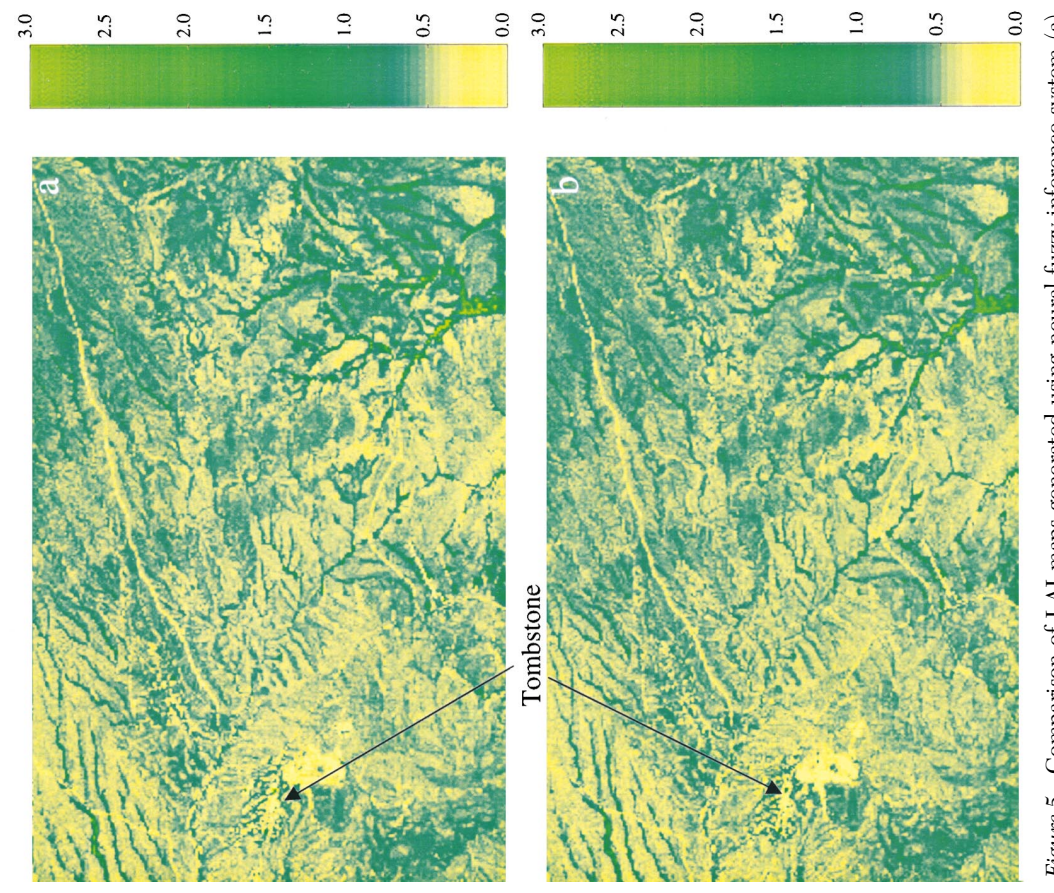
Figure 5. Comparison of LAI maps generated using neural fuzzy inference system (a) and LAI–SVI (b) techniques with TM image of 7 September 1990.
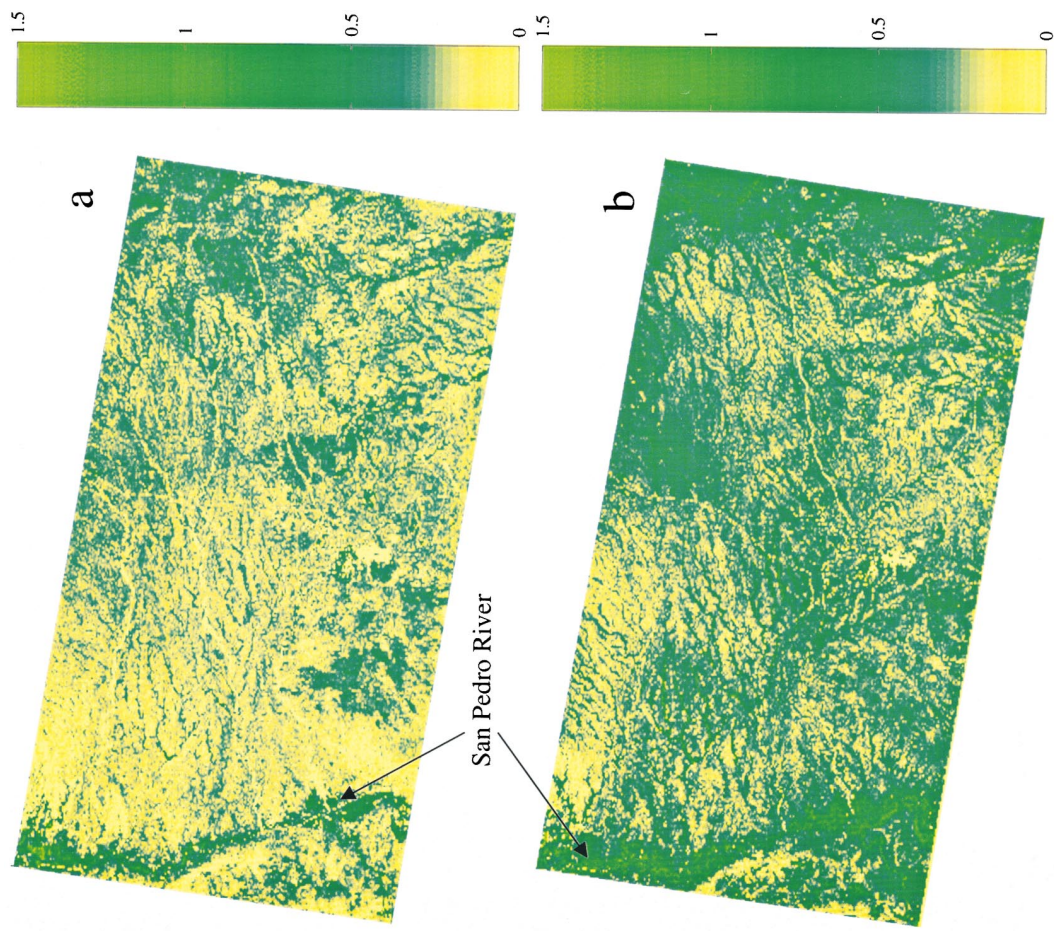

Figure 4. LAI maps generated with Landsat TM image acquired on April 22 (a) and September 7(b) 1990, using the proposed approach. These two dates represent vegetation status in the dry (a) and wet (b) seasons.
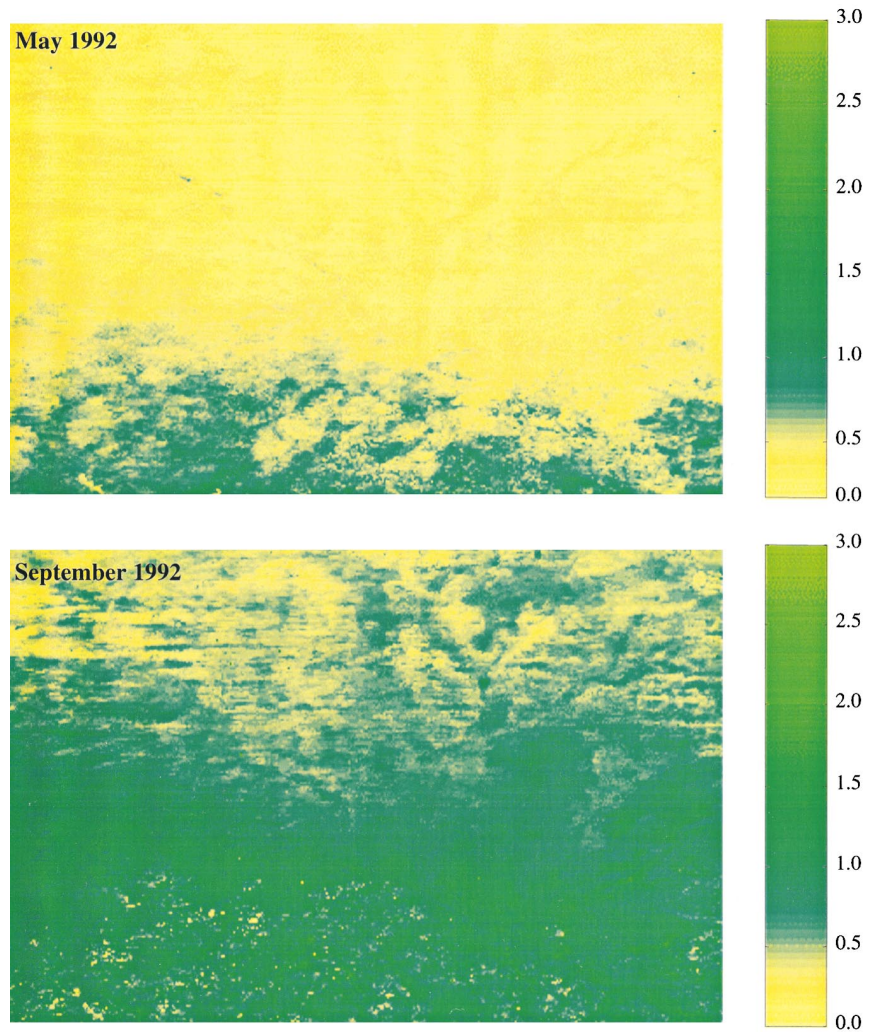
Figure 6. LAI distribution estimated using the proposed approach with AVHRR image composited for May (a) and September (b) 1992 over the Hapex-Sahel experimental site.

Therefore, the proposed approach appears to have produced reasonable estimates of LAI within this region.

In Figure 8a, the ground LAI measurements made at the South (S) site (13.24°N, 2.24°E) and Central West (CW) site (13.54°N, 2.51°E) during the Hapex-Sahel field campaigns are plotted as vertical bars, while the estimated LAI values from AVHRR data are plotted as solid lines as a function of day of year (DOY). There was good agreement between the estimated and measured LAI values up to DOY 280. Considering the differences in spatial sampling schemes of ground measurements and AVHRR spatial resolution (1.1 km), the results were reasonably satisfactory. The estimated LAI value on DOY 280 was underestimated by a factor of 50% (0.4 vs. 0.8) for the south Fallow site. At the Central West Fallow site, the estimated LAI values appeared to have been overestimated (Fig. 8a) (maximum difference was 0.18). Again, the vegetation sampling schemes and the larger spatial resolution of the AVHRR data might have contributed to these discrepancies.

LAI values were computed for the South Millet site from the 1992 AVHRR imagery. However, ground LAI measurements were made in 1993 only. Nevertheless, comparison of the temporal LAI dynamics (Fig. 8b) provided an indirect validation of the approach for Millet vegetation type for this site. Overall, the estimated LAI values were reasonably close to the ground measurements for all data from the Hapex-Sahel experimental sites.

To compare the results from this approach with those from other approaches such as the linear LAI-SVI by Asrar et al. (1985b), LAI maps were generated using 7 September 1990 TM images and compared in Figure 9. The spatial patterns were very similar, although the absolute LAI values may differ. To further examine the similarity and differences between the two approaches, randomly extracted data (10,000 pixels) from these two LAI maps are compared in Figure 10. When LAI<1.2, there was virtually no difference between the two approaches. However, they deviated from the 1:1 line significantly when LAI>1.2. The deviation from linear fit was due to the non-linear response of NDVI with LAI. However, in arid and semiarid regions, green leaf area
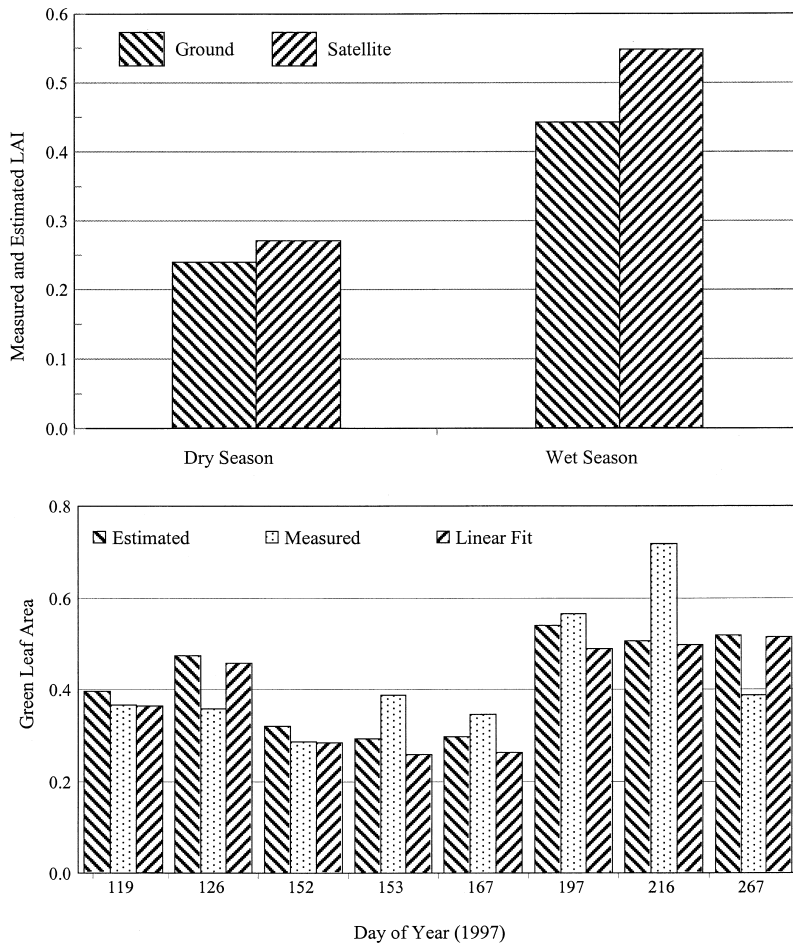
Figure 7. Comparison of estimated LAI from remote-sensing images with ground measurements collected at a) Walnut Gulch Experimental Watershed and b) the Audubon ranch.

index values are often small and, therefore, either approach is suitable.

CONCLUDING REMARKS

The proposed approach to estimating LAI using remote-sensing images was demonstrated to be reasonably satisfactory with the data from these experiments. The results from the proposed approach, with limited data sets, were similar to the linear empirical approach by Asrar et al. (1985b). This approach was promising in that it did not require laborious intensive ground LAI measurements. It relied only on multidirectional remote-sensing measurements from either space-based or ground-based sensing systems. Because this approach is independent of vegetation type, it can be applied easily to images acquired over large areas if the area of interest consists of the same or similar vegetation types. Therefore, use of a single LAI–SVI equation derived from one study site on geographically different areas should be cautious. In this study, the area of interest consisted primarily of desert grass or shrubs and, therefore, may not be suitable for areas of multiple vegetation types. One way to deal with multivegetation type areas is to generate vegetation classification maps first and apply this approach for each vegetation class (Running et al., 1996). Global use of this approach is therefore limited to areas of similar vegetation type and phenology.

The proposed approach requires that multiangular (either ground- or space-based) data be collected for the use in the inversion step in Figure 1. Measuring multidirectional reflectance data may be difficult in many cases. In this case, direct measurements of the required model parameters may be used instead.

Because of its robust nature and substantially reduced computation time, the proposed approach can be operationally implemented. Both LAI-SVI and neural fuzzy inference system techniques worked well with the data set used. The LAI-SVI technique can be easily understood, but interpretation of fuzzy inference system may be difficult, although they both can be used in generating large-scale LAI maps using remote-sensing images.

There are several comments about the proposed approach. First, no sensitivity analysis was conducted in this study to examine how noise levels inherent within remote-sensing images could have affected the accuracy of LAI estimation. In many cases, multidirectional remote-sensing images are compiled or mosaicked from
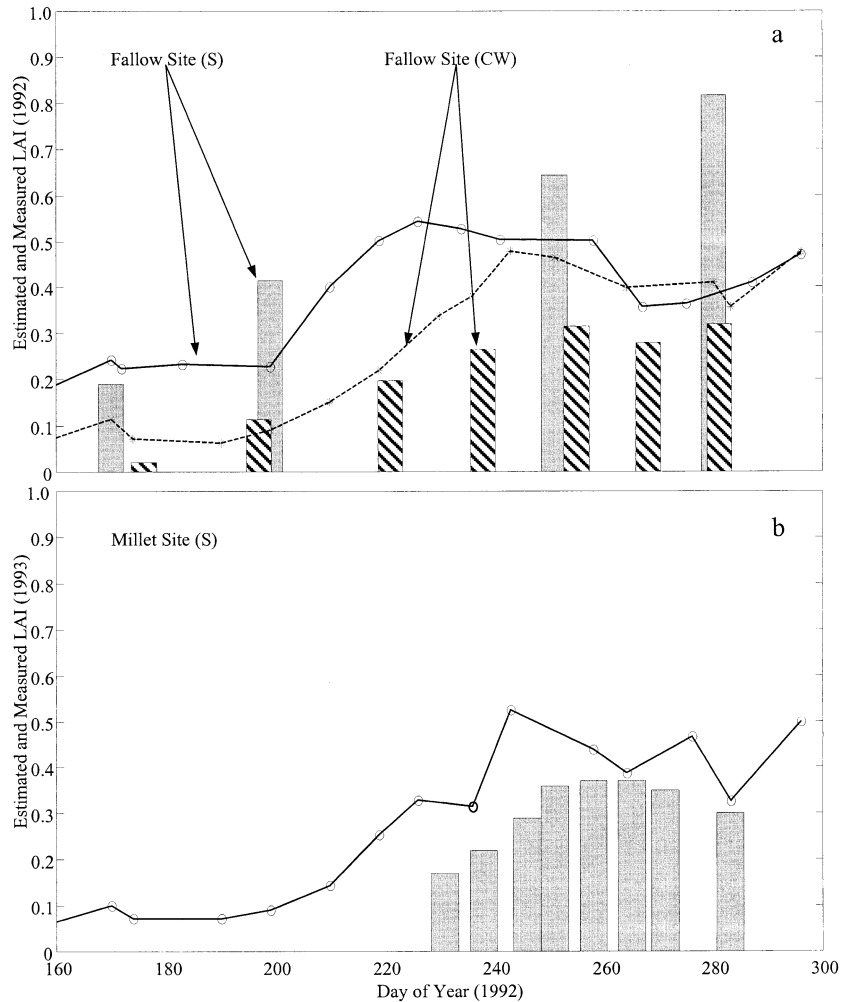
Figure 8. Comparison of temporal LAI values estimated using AVHRR data with ground measurements for a) Fallow (at the Central West and South Super sites) and b) Millet at the South Super site during the Hapex-Sahel experiment. Note that the LAI data for the Millet site (b) were measured in 1993, while the AVHRR data were acquired in 1992 at the same site.

several satellite overpasses after georeferencing and atmospheric corrections. If any of these images contain noise due to atmospheric perturbation, cloud contamination, and soil background variation, the model inversion may not perform well. In this case, it is suggested that these pixels be excluded in the quality control step by setting up a flag. In some cases, the noise level in satellite images may not be high enough to result in inversion failure, but high enough to result in substantial errors in estimated LAI values. One way to avoid this possible error is to ensure the data quality by removing these affected pixels or images.

A second comment is related to the LAI–SVI equation selection procedure used in this approach. Because the inversion is made with randomly selected pixels, the selected equation and its associated coefficients may be different each time the approach is used. This may be resolved by selecting a large representative number of pixels ($N=2500$ in this study) so that there is no significant difference between subsequent data sampling. Furthermore, other types of LAI–SVI equations may perform better for a particular data set than those listed in

this study. One should include as many types of equations as possible when using this approach. In addition, the spectral vegetation index used in this study was NDVI. As a number of studies indicated, the NDVI is subject to many external effects, particularly to soil background and atmospheric conditions. It is suggested that other indices be tested. The choice of NDVI in this study was made because this index has been used frequently in the past, and LAI–NDVI equations were proposed in numerous studies. Nevertheless, NDVI has been demonstrated to give satisfactory LAI estimates.

A third comment is related to bidirectional effects one may find in remote-sensing images. For the inversion process, the bidirectional information is critically important because BRDF models rely on this angular information for successful simulation and inversions. These bidirectional effects are no longer useful, however, after the inversion procedure is finished in Step 1. They may cause estimation errors, because vegetation indices such as NDVI are quite sensitive to view angles and solar positions. Therefore, the bidirectional effects may be propagated to influence LAI estimations when using the
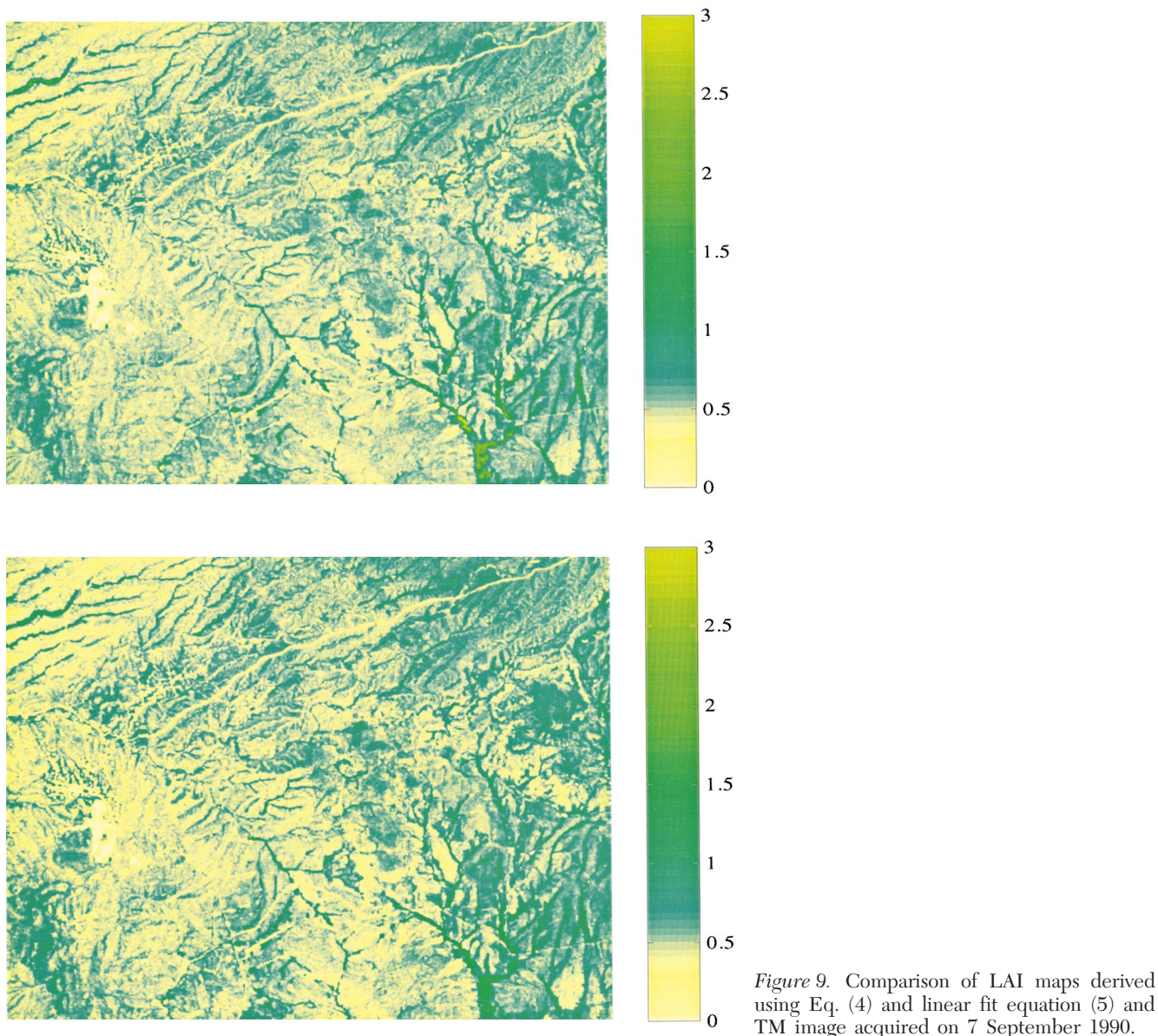
Figure 9. Comparison of LAI maps derived using Eq. (4) and linear fit equation (5) and TM image acquired on 7 September 1990.

LAI–SVI approach in Step 3. To avoid this type of error, the inversion can theoretically be done with the entire image (therefore, there is no need for statistical regression and equation selection). Doing so, however, may not only require unacceptable computation time, but also result in a substantial number of inversion failures. The inversion failure may result from noise in the satellite images as mentioned previously or from the lack of considerations of factors, such as topography in BRDF models. The topography should be considered in conjunction with the sensor's geometric configuration, but has not yet been incorporated into BRDF models. The bidirectional effects may not be a concern, however, with the neural fuzzy system approach (Step 3b in Fig. 1), because one can include the angular variables (view and solar zenith and azimuth angles, for example) in the training data set. The inclusion of angular variables may

improve the LAI estimation accuracy, because they provide additional information to train the fuzzy system. Therefore, the neural fuzzy system approach may be preferable to the LAI–SVI approach in Step 3.

Finally, the accuracy in LAI estimation depends on the accuracy of BRDF models used. In the SAIL model used in this study, the soil background was treated as a Lambertian surface. This assumption may have contributed to the discrepancies found in this study. Use of other models, such as PROSPECT (Jacquemoud, 1993), need to be explored. It should also be pointed out that the proposed approach can be used to estimate other physical parameters such as leaf optical properties and vegetation geometric structure parameters by inverting physically based models. Again, the neural fuzzy system may have advantages over the equation-based approach, because there are not many established equations linking
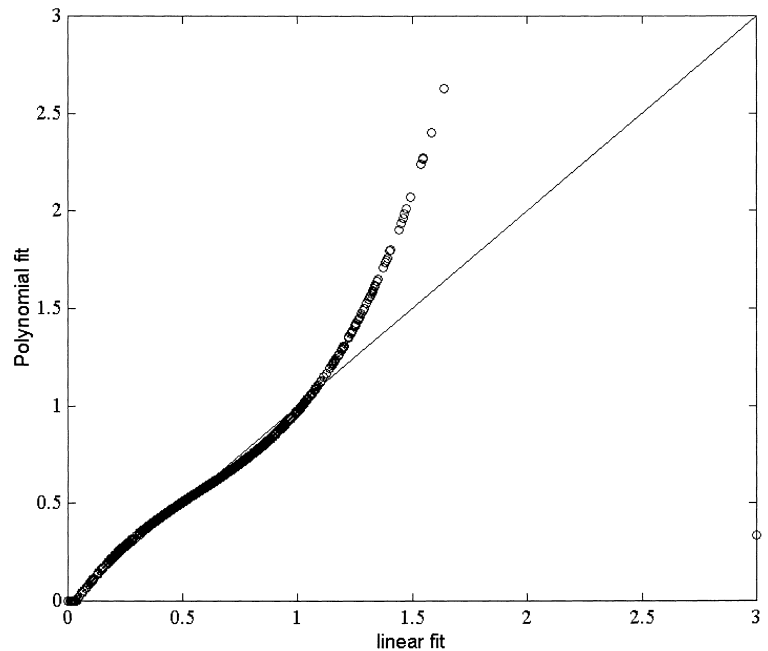
Figure 10. Comparison of polynomial fit obtained from this study with a linear fit from Asrar et al. (1985b).

biophysical parameters to remotely sensed variables. Use of this approach for other biophysical variables is logically feasible, but remains to be tested.

REFERENCES

Asrar, G., Kanemasu, E. T., Jackson, R. D., and Pinter, P. J., Jr. (1985a), Estimation of total above-ground phytomass production using remotely sensed data. *Remote Sens. Environ.* 17:211–220.

Asrar, G., Kanemasu, E. T., and Yoshida, M. (1985b), Estimates of leaf area index from spectral reflectance of wheat under different cultural practices and solar angle. *Remote Sens. Environ.* 17:1–11.

Baret, F. (1995), Use of spectral reflectance variation to retrieve canopy biophysical characteristics. In *Advances in Environmental Remote Sensing* (M. Darson and S. Plummer, Eds.), John Wiley and Sons, Inc., pp.33–51.

Best, R. G., and Harlan, J. C. (1985), Spectral estimation of green leaf area index of oats. *Remote Sens. Environ.* 17: 27–36.

Burgess, D. W., and Pairman, D. (1997), Bidirectional reflectance effects in NOAA AVHRR data, *Int. J. Remote Sens.* 18:2815–2825.

Clevers, J. G. P. W. (1989), The application of a weighted infrared-red vegetation index for estimating leaf area index. *Remote Sens. Environ.* 29:25–37.

Curran, P. J. (1983), Multispectral remote sensing for the estimation of green leaf area index. *Phil. Trans. Roy. Soc. London Ser. A* 309:257–270.

Deering, D. W. (1989), Field measurements of bidirectional reflectance. In *Theory and Applications of Optical Remote Sensing* (G. Asrar, Ed.), John Wiley and Sons, Inc., pp. 14–65.

Goel, N. S., and Deering, D. W. (1985), Evaluation of a canopy reflectance model for LAI estimation through its inversion. *IEEE Trans. Geosci. Remote Sens.* GE-23:674–684.

Goel, N. S., and Grier, T. (1987), Estimation of canopy parameters of row planted vegetation canopies using reflectance data for only four views. *Remote Sens. Environ.* 21:37–51.

Goel, N. S., and Thompson, R. L. (1984a), Inversion of vegetation canopy reflectance models for estimating agronomic variables. IV. Total inversion of the SAIL model. *Remote Sens. Environ.* 15:237–253.

Goel, N. S., and Thompson, R. L. (1984b), Inversion of vegetation canopy reflectance models for estimating agronomic variables V: Estimation of LAI and average leaf angle using measured canopy reflectances. *Remote Sens. Environ.* 16: 69–85.

Goutorbe, J. P., Lebel, T., Tinga, A., et al. (1994), Hapex-Sahel: a large scale study of land–atmosphere interactions in the semi-arid tropics. *Ann. Geophys.* 12:53–64.

Holben, B. N., and Justice, C. O. (1980), The topographic effect on spectral response from nadir-pointing sensors. *Photogrammetric Engineering and Remote Sensing* 46:1191.

Huete, A. R. (1988), A soil-adjusted vegetation index (SAVI). *Remote Sens. Environ.* 25:295–309.

Huete, A. R. (1989), Soil influences in remotely sensed vegetation-canopy spectra. In *Theory and Applications of Optical Remote Sensing* (G. Asrar, Ed.), John Wiley and Sons, Inc., pp. 107–141.

Huete, A. R., Hua, G., Qi, J., Chehbouni, A., and van Leeuwen, W. J. D. (1992), Normalization of multidirectional red

and NIR reflectances with the SAVI. *Remote Sens. Environ.* 41:143–154.

Jackson, R. D., Teillet, P. M., Slater, P. N., et al. (1990), Bidirectional measurements of surface reflectance for view angle corrections of oblique imagery. *Remote Sens. Environ.* 32:189–202.

Jacquemoud, S. (1993), Inversion of the PROSPECT+SAIL canopy reflectance models from AVIRIS equivalent spectra: theoretical study. *Remote Sens. Environ.* 44:281–292.

Jacquemoud, S., Baret, F., Andrieu, B., Danson, F. M., and Jaggard, K. (1995), Extraction of vegetation biophysical parameters by inversion of the PROSPECT+SAIL models on sugar beet canopy reflectance data. Applications to TM and AVIRIS sensors. *Remote Sens. Environ.* 52:163–172.

Justice, C. O., Wharton, S. W., and Holben, B. N. (1981), Application of digital terrain data to quantify and reduce the topographic effect on Landsat data. *Int. J. Remote Sens.* 2:213–230.

Kaufman, Y. J. (1989), The atmospheric effect n remote sensing and its correction. In *Theory and Applications of Optical Remote Sensing* (G. Asrar, Ed.), John Wiley and Sons, Inc., pp. 336–428.

Kaufman, Y. J., and Tanré D. (1992), Atmospherically resistant vegetation index (ARVI) for EOS-MODIS. *IEEE Trans. Geosci. Remote Sens.* 30:261–270.

Kerr, Y. H. (1994), *Hapex-Sahel Information System*, CD-ROMs, CESBIO, Toulouse, France.

Kimes, D. S., Newcomb, W. W., Tucker, C. J., et al. (1985), Directional reflectance factor distributions for cover types of Northern Africa. *Remote Sens. Environ.* 18:1–19.

Kustas, P. W., Goodrich, D. C., Moran, S. M., et al. (1991), An interdisciplinary field study of the energy and water fluxes in the atmosphere–biosphere system over semiarid rangelands: description and some preliminary results. *Bull. Am. Meteorol. Soc.* 72:1683–1705.

Moran, M. S., Jackson, R. D., Clarke, T. R., et al. (1996), Reflectance factor retrieval from Landsat TM and SPOT HRV data for bright and dark targets. *Remote Sens. Environ.* 52:218–230.

Peterson, D. L., Spanner, M. A., Running, S. W., and Teuber, K. B. (1987), Relationship of thematic mapper simulator data to leaf area index of temperate coniferous forest. *Remote Sens. Environ.* 22:323–341.

Pinter, P. J., Jr., Kelly, H. L., Jr., and Schnell, S. (1987), Spectral estimation of alfalfa biomass under conditions of variable cloud cover. In *18th Conference of Agricultural and Forest Meteorology*, 15–18 September, Purdue University, W. Lafayette, IN, pp. 83–86.

Pinty, B., and Verstraete, M. M. (1992), GEMI: a non-linear index to monitor global vegetation from satellites. *Vegetatio* 101:15–20.

Pinty, B., Verstraete, M. M., and Dickinson, R. E. (1990), A physical model of the bidirectional reflectance of vegetation canopies 2. Inversion and validation. *Journal of Geophysical Research* 95(D8):11,767–11,775.

Price, J. C., and Bausch, J. C. (1995), Leaf area index estimation from visible and near-infrared reflectance data. *Remote Sens. Environ.* 52:55–65.

Prince, S. D., Kerr, Y. H., Goutorbe, J. P., et al. (1995), Geographical, biological and remote sensing aspects of the hydrologic atmospheric pilot experiment in the Sahel (Hapex-Sahel). *Remote Sens. Environ.* 51:215–234.

Qi, J., Huete, A. R., Moran, M. S., Chehbouni, A., and Jackson, R. D. (1993), Interpretation of vegetation indices derived from multi-temporal SPOT images. *Remote Sens. Environ.* 44:89–101.

Qi J., Kerr, Y., and Chehbouni, A. (1994a), External factor consideration in vegetation index development. In *Sixth International Symposium on Physical Measurements and Signatures in Remote Sensing*, 17–21 January, CNES, Toulouse, France, pp. 723–730.

Qi, J., Huete, A. R., Cabot, F., and Chehbouni, A. (1994b), Bidirectional properties and utilizations of high resolution spectra from a semi-arid watershed. *Water Resour. Res.* 30:1271–1279.

Qi, J., Chehbouni, A., Huete, A. R., Kerr, Y., and Sorooshian, S. (1994c), A modified soil adjusted vegetation index (MSAVI). *Remote Sens. Environ.* 48:119–126.

Qi, J., Cabot, F., Moran, M. S., and Dedieu, G. (1995), Biophysical parameter retrievals using multidirectional measurements. *Remote Sens. Environ.* 54:71–83.

Rahman, H., and Dedieu, G. (1994), SMAC: a simplified method for the atmospheric correction of satellite measurements in the solar spectrum. *Int. J. Remote Sens.* 15:123–143.

Roujean, J. L., Leory, M., Podaire, A., and Deschamps, P. Y. (1992), Evidence of surface reflectance bidirectional effects from a NOAA/AVHRR multi-temporal data set. *Int. J. Remote Sens.* 13:685–698.

Running, S. W., Myneni, R. B., Nemani, R., and Glassy, J. (1996), MODIS LAI (Leaf Area Index), Algorithm Theoretical Basis Document, 1 November, NASA/Goddard Space Flight Center, Code 900, Greenbelt, MD.

Verhoef, W. (1984), Light scattering by leaf layers with application to canopy reflectance modeling, the SAIL model. *Remote Sens. Environ.* 16:125–141.

Vermote, E., Tanré, D., and Herman, M. (1990), Atmospheric effects on satellite imagery: correction algorithms for ocean color or vegetation monitoring. *Int. Soc. Photogramm. Remote Sens.* 28:46–55.